J Supercond Nov Magn (2011) 24:2189–2201
DOI 10.1007/s10948-011-1180-y

ORIGINAL PAPER

The Effects of Sb Substitution on Structural Properties in $YBa_2Cu_3O_7$ Superconductors

Gönül B. Akyüz · Kemal Kocabaş · Aylin Yıldız · Lütfi Özyüzer · Muhsin Çiftçioğlu

Received: 7 April 2011 / Accepted: 26 April 2011 / Published online: 19 May 2011

Abstract In this study, the effects of partial Sb^{3+} ion substitutions for the Y sites and the Cu sites on the superconducting properties of $YBa_2Cu_3O_y$ (Y123) ceramic superconductors were investigated. The samples were prepared by the conventional solid-state reaction method and the properties of the samples were investigated by means of X-ray diffraction, AC magnetic susceptibility measurements, scanning electron microscope, and energy dispersive X-ray analysis. The critical temperatures were determined to be in the range of 80–92 K for both Systems I and II. It was found that Sb-addition leads to the formation of the non-superconducting YBa_2SbO_6 phase, which has a negative effect on the critical temperature, since the highest critical temperature was measured for pure Y123. However, the increasing substitution level has a negligible effect on the X-ray diffraction analysis peak intensities of the superconducting phases. In addition, SEM images showed that Sb substitution decreases the grain size and modifies the microstructure development, which makes the samples denser.

Keywords Y-based cuprates · Effects of substitution · SEM

G.B. Akyüz (✉)
Physics Department, Adnan Menderes University, 09100 Aytepe, Aydın, Turkey
e-mail: gonulbilgec@gmail.com

K. Kocabaş · A. Yıldız
Faculty of Science, Physics Department, Dokuz Eylül University, 35160 Buca, İzmir, Turkey

L. Özyüzer
Department of Physics, İzmir Institute of Technology, 35430 Urla, İzmir, Turkey

M. Çiftçioğlu
Chemical Engineering Department, İzmir Institute of Technology, 35430 Urla, İzmir, Turkey

1 Introduction

Lanthanum barium copper oxide (LBCO), which has a critical temperature (T_c) of 35 K, was the first high-T_c superconductor (HTS) discovered by Bednorz and Müller [1]. Chu and co-workers [2] increased the transition temperature of HTSs to around 92 K by replacing Y^{3+} ions with La^{3+} thus forming $YBa_2Cu_3O_7$(Y123). Y123 is the first material found to have a superconducting transition temperature above liquid nitrogen temperature. After this discovery, the Y-Ba-Cu-O family of compounds, like Y123, $YBa_2Cu_4O_8$ (Y124, $T_c = 80$ K) and $YBa_2Cu_4O_7$ (Y247, $T_c = 40$ K), have been intensively studied [2–4]. Meanwhile, numerous papers have been published on the effects of the addition of various elements into the Y123 structure for further improvement in T_c, critical current, pinning, etc. [5–10]. A recently synthesized new Y-based HTS, $Y_3Ba_5Cu_8O_{18}$(Y358), exhibited superconductivity above 100 K [11]. In the previous studies of our group, several types of substitution studies were also done to improve the desired high-T_c phase [12–15]. Research on doping or substitution of other elements into cuprate superconductors not only contributes to the find of applications for superconductivity but also helps to determine the pairing mechanism in HTSs.

The planes containing copper and oxygen atoms that are chemically bonded to each other have a crucial importance in Y123. The special nature of the copper-oxygen chemical bond contributes to an effective electrical conductivity in certain directions. The existence of the Cu-O chains and the CuO_2 planes in cuprate superconductors indicates the important role of Cu atoms. Thus, the ionic radius as well as the valance number of the dopant element has a crucial role in determining the characteristics of new superconductors.

Doping of Y123 with various elements is conducted for two basic purposes. The first one is the modification of the

microstructure in order to obtain fundamental information related to the possible mechanisms, and the second one is to improve its physical characteristics. In order to improve the superconducting properties of Y123, rare earth element doping of the Y site has been investigated [16–23]. It was shown that substitutions at the Y and Ba sites did not generate any discernible effect, while substitution at the Cu and O sites had significant effects on the superconducting properties of cuprates [24]. The cation doping of both the Cu-O chains and the CuO_2 planes in $YBa_2Cu_{3-x}M_xO_y$ ceramics is still a field of considerable interest. Numerous studies have been performed in order to gain more information about the role of each Cu site on the structural and physical properties of Y123 superconductors. Doping with several metals and metal oxides, such as CeO_2, Lu, Zn, Ca have been reported to lead to the formation of non-superconducting phases and, as a result, to a decrease in the critical temperature of Y123 [25, 26]. Therefore, the selection of the doping elements is limited. However, due to the low melting point and the possible surfactant action of semi-metallic Sb_2O_3 doping, it is expected that doping with Sb could improve the grain boundary characteristics and enhance the intergranular coupling in Y123. Paulose et al. [22] reported that Sb_2O_3 doping significantly increases the rate of oxygen absorption in the Y123 system. In addition, Jin et al. [20] determined that 5% Sb_2O_3 doping of Y123 improves the value of the critical current density, J_c, along with a decrease in T_c and a reduction in grain size with increasing porosity. Furthermore, Vlakhov [21] reported that even small doping levels of Sb shift the step of $J_c(B)$ dependence to higher magnetic fields but cannot improve the weak link behavior.

In the present study, the effects of partial Sb substitution for Y and Cu sites on the superconducting properties of Y123 superconductors were investigated. The properties of $Y_{1-x}Sb_xBa_2Cu_3O_y$ (System I) and $YBa_2Cu_{3-x}Sb_xO_y$ (System II) ($x = 0.00$, 0.05, 0.10, 0.15, 0.20) specimens, where Sb was added in the form of Sb_2O_3, were investigated with related changes in the microstructure and related dynamic processes; AC susceptibility measurements, X-ray diffraction (XRD), and energy-dispersive X-ray (EDAX) analysis, scanning electron microscope (SEM) imaging and density-porosity measurements.

2 Experimental Procedures

The ceramic superconducting samples of $Y_{1-x}Sb_xBa_2Cu_3O_y$ (System I) and $YBa_2Cu_{3-x}Sb_xO_y$ (System II) samples were synthesized by the conventional solid state reaction technique. High-purity powders of Y_2O_3(99.99%), $BaCO_3$(99.99%), Sb_2O_3(99.99%), and CuO(99.99%) were mixed in appropriate molar ratios to give $x = 0.00$, 0.05, 0.10, 0.15, and 0.20 (Coded as A, B, C, D, E, respectively, for Systems I and II). These powders were finely ground using a mortar and pestle and calcined at 900 °C for a period of 15 hours in a furnace (Nabertherm) in air atmosphere initially. The calcined powders were reground and recalcined under the above conditions to achieve completion of the following reaction:

$$0.5Y_2O_3 + 2BaCO_3 + 3CuO \rightarrow YBa_2Cu_3O_{6.5} + 2CO_2. \quad (1)$$

A gray-black powder was obtained after the second calcination process. The powders were ground again and uniaxially pressed to form 13 mm diameter and 1.5 mm thick pellets under a pressure of 500 MPa. These pellets were sintered in a Protherm PTF 12/50/450 model tube furnace at 940 °C for 20 hours in an air atmosphere. Both the heating and cooling rates were approximately 7.7 °C/min.

The lattice parameters, phase structures and impurities in the samples along with the oxygen contents were calculated by using the length of the c-axis as determined from XRD patterns. X-ray powder diffraction measurements were made in the range of $2\theta = 20°$–$70°$ with a CuK_α radiation source using an X'Pert Pro Philips Analytical Diffractometer. These results were analyzed using the Powder Diffraction Programme (PDP) in order to determine the lattice parameters (a, b, c) of the samples.

The critical temperatures, diamagnetic transitions, and sample quality were determined by the AC susceptibility measurements performed in the temperature interval of 78 to 102 K using an AC magnetic field with a frequency of 1 kHz.

SEM micrographs were analyzed to understand the microstructure, the size and orientation of the superconducting grains, and pores between them. These analyses of the top and fractured surfaces of the samples were analyzed by scanning electron microscope (Philips XL-30S FEG). The elemental composition and the possible incorporation of impurities in various regions of the samples were qualitatively checked by EDAX using the same system. Finally, the densities of the samples were measured using a density measurement kit (Sartorius) based on Archimedes water displacement technique. These density results allowed us to calculate the porosity (the degree of granularity) for each sample, which gives valuable information about the strength of connection between superconducting grains.

3 Results and Discussion

3.1 System I

In this section, the results obtained on the effects of Sb substitution for Y in the $Y_{1-x}Sb_xBa_2Cu_3O_y$ (System I) with

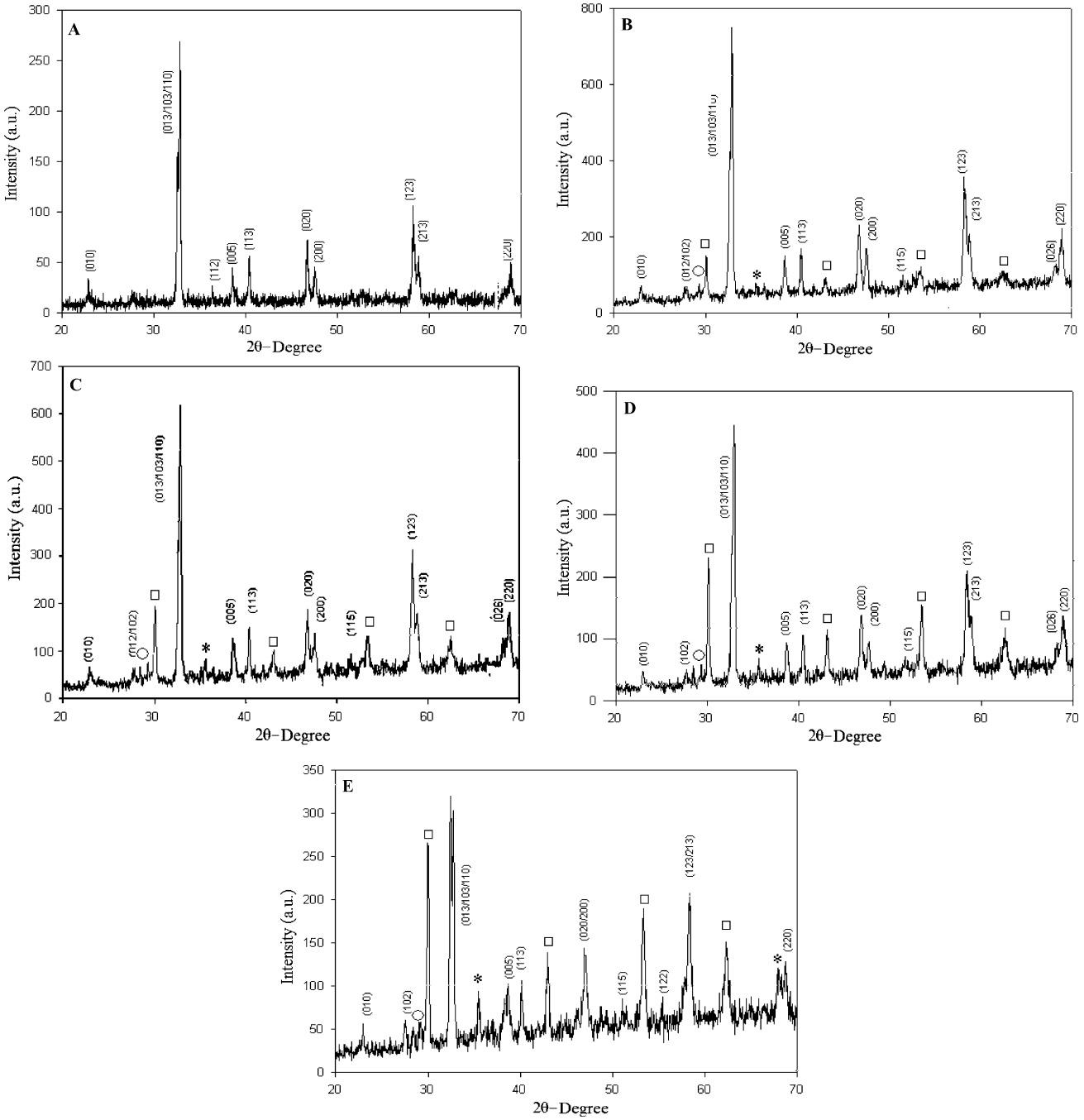

Fig. 1 XRD patterns of samples **A**, **B**, **C**, **D**, and **E** with the composition of $Y_{1-x}Sb_xBa_2Cu_3O_y$ ($x = 0.00$–0.20) (□ YBa_2SbO_6 phase, ∗ CuO phase, ◯ $BaCuO_2$ phase)

A ($x = 0.0$), B ($x = 0.05$), C ($x = 0.10$), D ($x = 0.15$), and E ($x = 0.20$) are presented and discussed. The XRD patterns of all the samples in System I are given in Fig. 1. The characteristic peaks of the Y123 phase were determined by using the tables given by Bell [27]. Deviations in the lattice parameters (a, b, c) with Sb doping content (x) were insignificant and all the samples had a multiphase nature with orthorhombic main Y123 phase. However, the lattice parameter of this system samples changed due to the difference in ionic radius between Y^{3+} (0.90 Å) and Sb^{3+} (0.76 Å). Additional peaks were observed at $2\theta = 30.06°$, 43.10°, 53.60°, and 62.40° with increasing doping level, indicating the presence of additional phases. YBa_2SbO_6, $BaCuO_2$ phases, and CuO peaks with small intensities have been identified in the doped samples. The $BaCuO_2$ impurity, which is a characteristic phase for Y123 compounds prepared by the solid-

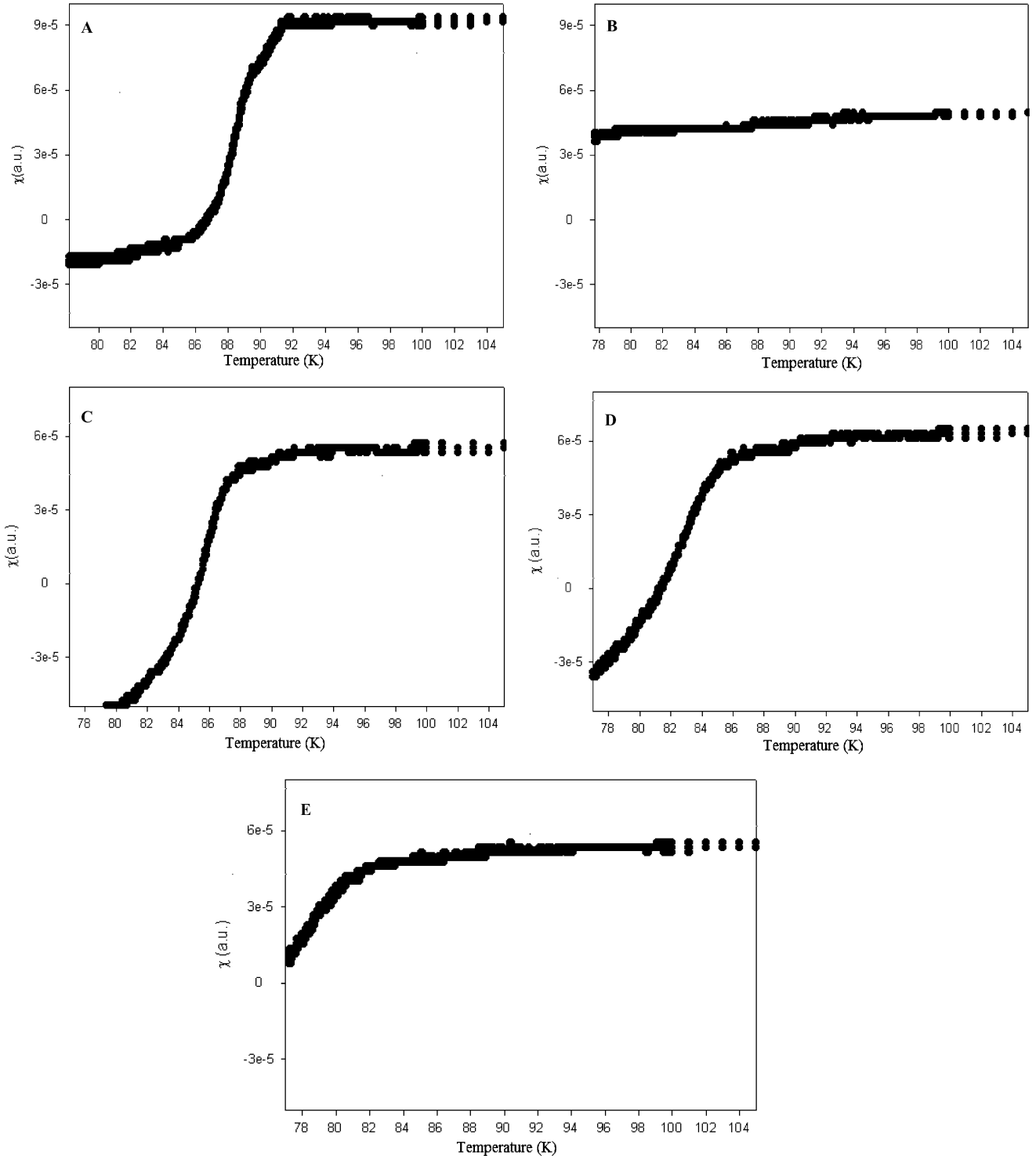

Fig. 2 Temperature dependence of the real part AC susceptibility of the samples Y_xSb_{1-x} $Ba_2Cu_3O_y$ $(0.05 \leq x \leq 0.20)$

state reaction method, has been detected at $2\theta = 29.30°$ in these samples. There was an indication Sb is present in the Y123 lattice, since we could detect the peaks of Sb containing phases from the EDAX analysis. The oxygen contents (y) of all the samples were also determined by using the approximate relationship between the lattice constant y and c ($y = 7 - ((c - 11.68)/0.1501)$) given in [28]. The oxygen contents (y) determined by this relationship in the System I samples were nearly 7 in all cases, however no oxygen enrichment of the atmosphere was not made during heat treatments.

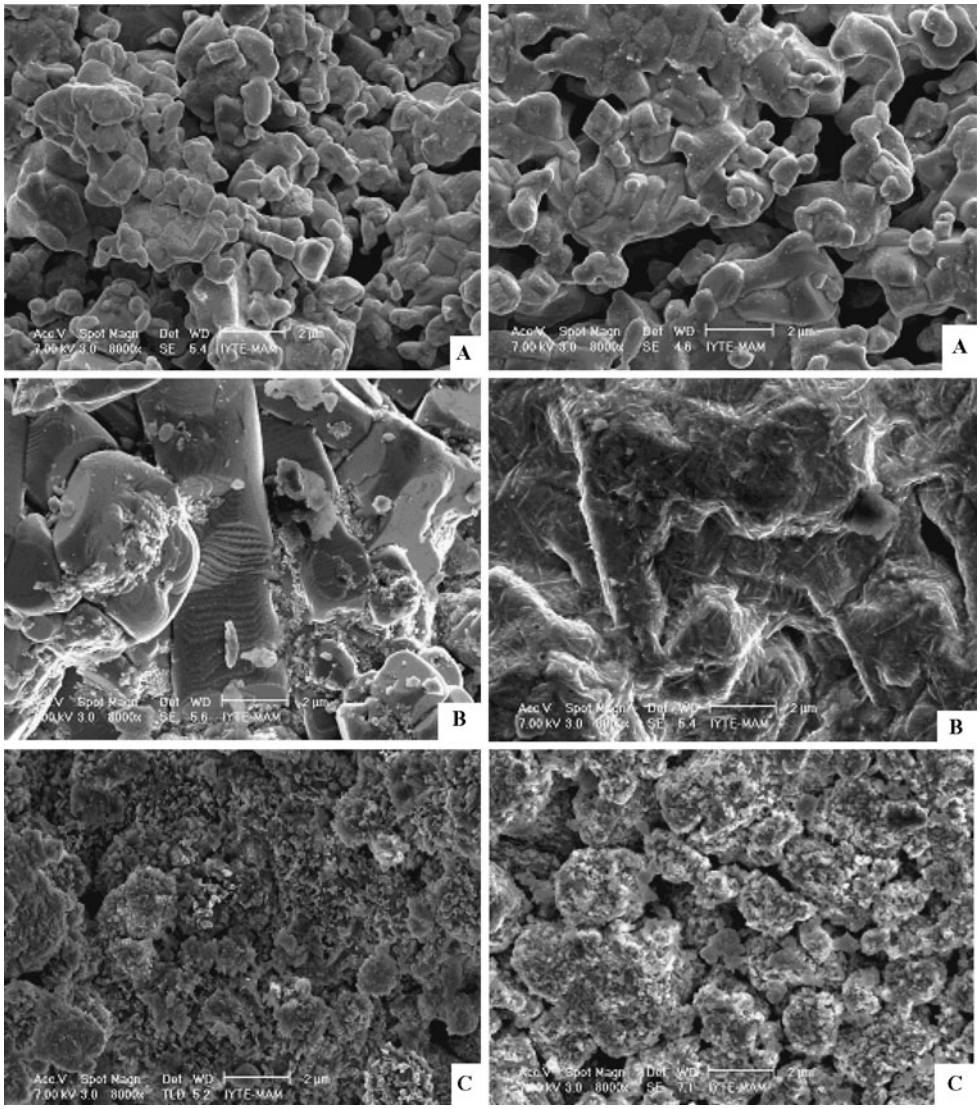

Fig. 3 SEM images of the samples $Y_{1-x}Sb_xBa_2Cu_3O_y$ with (**A**) $x = 0.00$, (**B**) $x = 0.05$, (**C**) $x = 0.10$, (**D**) $x = 0.15$, and (**E**) $x = 0.20$, respectively. *Left column* shows fracture surface while *right column* shows top surface of samples, respectively

The real and imaginary parts of the AC susceptibility of the $Y_{1-x}Sb_xBa_2Cu_3O_y$ ($x = 0, 0.05, 0.10, 0.15, 0.20$) superconductors were measured using a mutual inductance measurement system with lock-in amplifier (Stanford Research Systems Model SR830 DSP) under a magnetic field with constant frequency (1 kHz) and amplitude. The results for the real part of the AC susceptibility of System I samples as a function of temperature are shown in Fig. 2.

The variations of $T_{c,(onset)}$ and $T_{c,(R=0)}$ with Sb substitution content are further shown in this figure. Basically, almost the same behavior is seen for all the samples in System I. The curves show two graded drops occurring below the critical temperature. The first drop ($T_{c,(onset)}$) corresponds to the intrinsic properties of the grains, while the low-temperature step is associated with the occurrence of superconductivity at the grain boundaries. A critical temperature ($T_{c,(onset)}$) of about 92 K was observed for undoped sample ($x = 0.00$) from this susceptibility results. This critical temperature value which is obtained for pure samples prepared under solid-state reaction is an agreement with the literature [2, 18]. $T_{c,(onset)}$ value was measured as 88 K for sample C indicating a strong connectivity between the grains. Samples D and E showed a diamagnetic transition at 86 and 82 K, respectively. However, a diamagnetic transition was not observed for sample B, until the liquid nitrogen temperature and it was not possible to determine the $T_{c,(onset)}$ and $T_{c,(R=0)}$ in sample B and also $T_{c,(R=0)}$ in sample E.

The SEM photographs of the top surfaces as well as the fracture surfaces of all pellet microstructures are shown at 8000-X magnification in Fig. 3. The pure YBCO sample has a fine crystalline homogeneous structure that consists of almost spherical grains. The grain size decreases with a denser alignment of grains with increasing level of substitution, as also reported by Jin et al. [20]. The grains in all the samples seem to be randomly oriented. It is clear that the grain boundaries are likely to have weak links, and consequently

Fig. 3 (*Continued*)

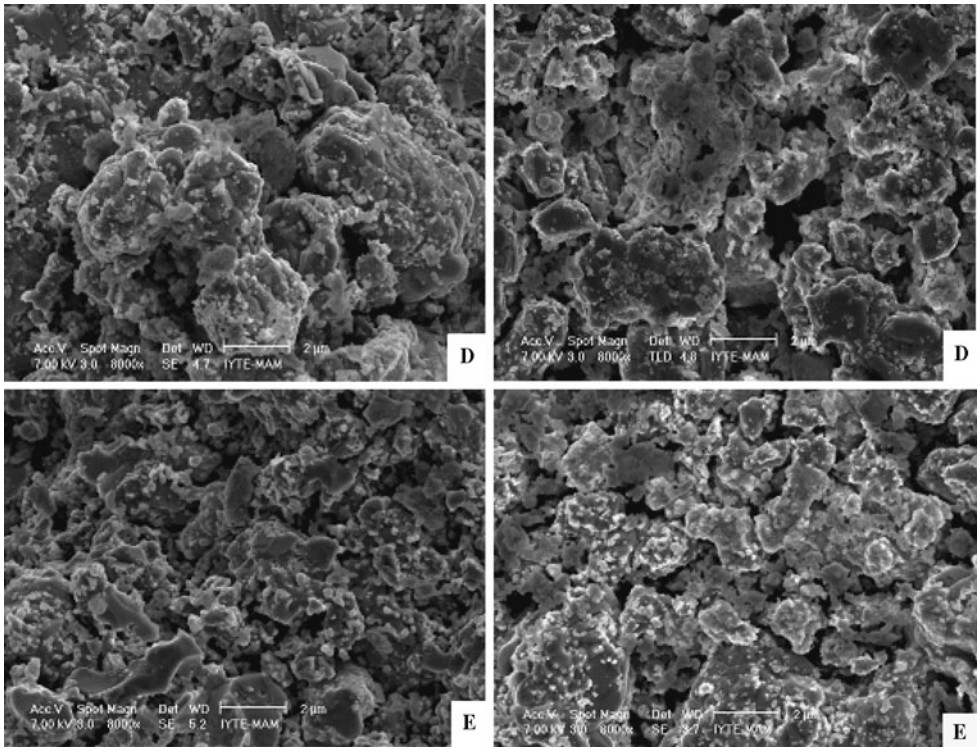

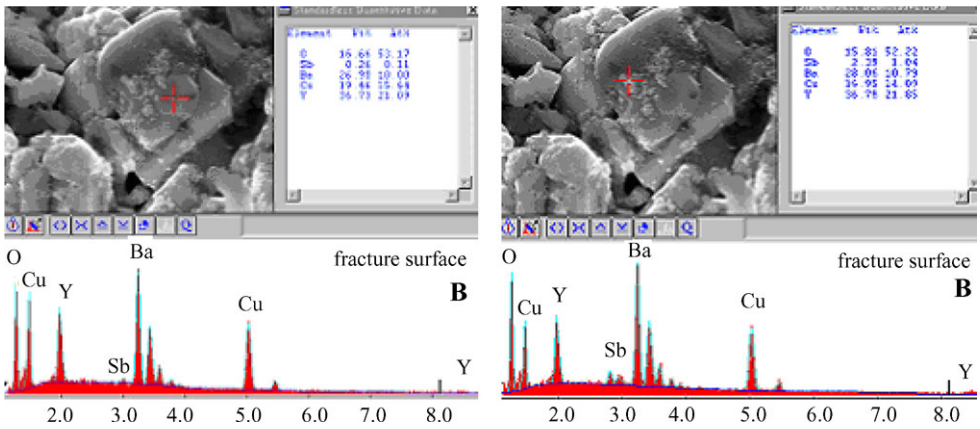

Fig. 4 (Color online) EDAX analysis results for two different regions of **B** samples in System I in their fracture surface

reduced intergranular coupling. While it was not possible to determine the grain sizes exactly, these microphotographs clearly demonstrated that the samples were porous. The homogeneity in the system was gradually lost with increasing Sb substitution level with a significant microstructure evolution. There were significant differences in the microstructures of the top and fracture surfaces of sample B with relatively large grains in the bulk of the sample (Fig. 3). A large number of fine particles along with relatively large irregular particles can be identified in the micrograph of sample B (Fig. 4). This can be attributed to a weak connectivity between the superconducting grains. Furthermore, along with the spherical plate-like grains, needle-like grains can also be easily identified in the sample C, D, and E micrographs. The EDAX analysis showed that these needle-like lumps, determined to correspond to Sb-rich regions, were visible in all micrographs but were especially evident in higher numbers in sample B (Fig. 4). The domination of lumps in sample B indicates the unfavorable effect on superconductivity. The plate-like grain size seems to increase in samples C and D, while it is the smallest in sample E (Fig. 3). These results are also in agreement with critical temperature values and XRD patterns. The EDAX analysis results shown in Figs. 5 and 6 further demonstrate the presence of YBa_2SbO_6 and CuO phases in samples C and E.

The density and porosity of System I samples are given in Table 1. The relative densities of the $Y_{1-x}Sb_xBa_2Cu_3O_y$ samples (as a percentage of the pure Y123 theoretical density of 6.357 g/cm^3) determined by the Archimedes water displacement method were 90.77% for $x = 0.00$, 88.09%

Table 1 The critical temperatures ($T_{c,(onset)}$–$T_{c,(R=0)}$), lattice parameters, oxygen content, density (ρ) and porosity (P) of the $Y_{1-x}Sb_xBa_2Cu_3O_y$ ($0.05 \leq x \leq 0.20$) samples

System I x	$T_{c,(onset)}$ (K)	$T_{c,(R=0)}$ (K)	$y(c)$	ρ (g/cm^3)	P (%)
0.00	92	90	6.995	5.77	9.27
0.05	–	–	6.995	5.60	11.97
0.10	88	86	6.995	5.61	11.79
0.15	86	82	6.995	5.84	8.04
0.20	82	–	6.996	5.89	7.42

for $x = 0.05$, 88.25% for $x = 0.10$, 91.87% for $x = 0.15$ and 92.65% for $x = 0.20$. The density and porosity results are listed in Table 1 and plotted with respect to Sb molar doping ratio (x) in Fig. 7. It is seen from Fig. 7 that the density decreases slightly for $x < 0.10$ Sb^{3+} concentration and it increases again for the D and E samples of System I with respect to the pure Y123 system. The porosities of the samples were calculated by using two methods described in [29, 30]. Porosity measurements help to identify the transport properties of the grain boundaries and the porosity results show that the pores are larger especially in sample B. The suppression of the diamagnetic signal in the susceptibility curve with decreasing critical temperature of sample B can be attributed to both the high porosity and the secondary phases observed in EDAX and SEM images as discussed before. The large pores indicate a week connection between the superconducting grains that can be minimized by use of the appropriate pellet consolidation pressure. Meanwhile, both density and porosity results suggest that the developing impurity phases containing Cu and Sb reduced the pore content in samples D and E and eventually cause the formation of denser samples.

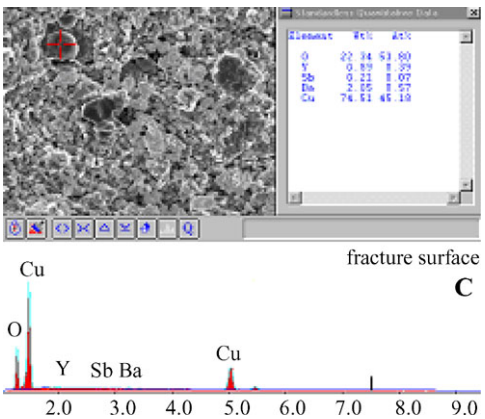

Fig. 5 (Color online) The presence of Cu atoms as CuO at different regions in the fracture surface of the sample C in System I

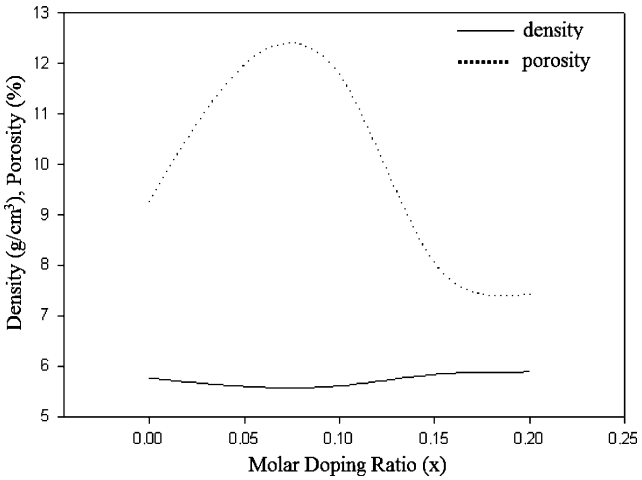

Fig. 7 Variation of the density and porosity of Sb doped $Y_{1-x}Sb_xBa_2Cu_3O_y$ ($0.05 \leq x \leq 0.20$) samples

Fig. 6 (Color online) YBa_2SbO_6 and CuO phases observed in sample E for the System I

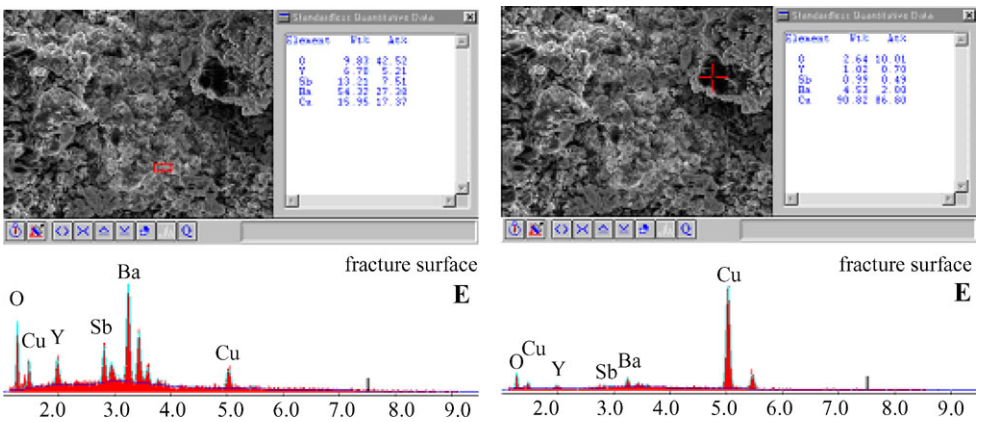

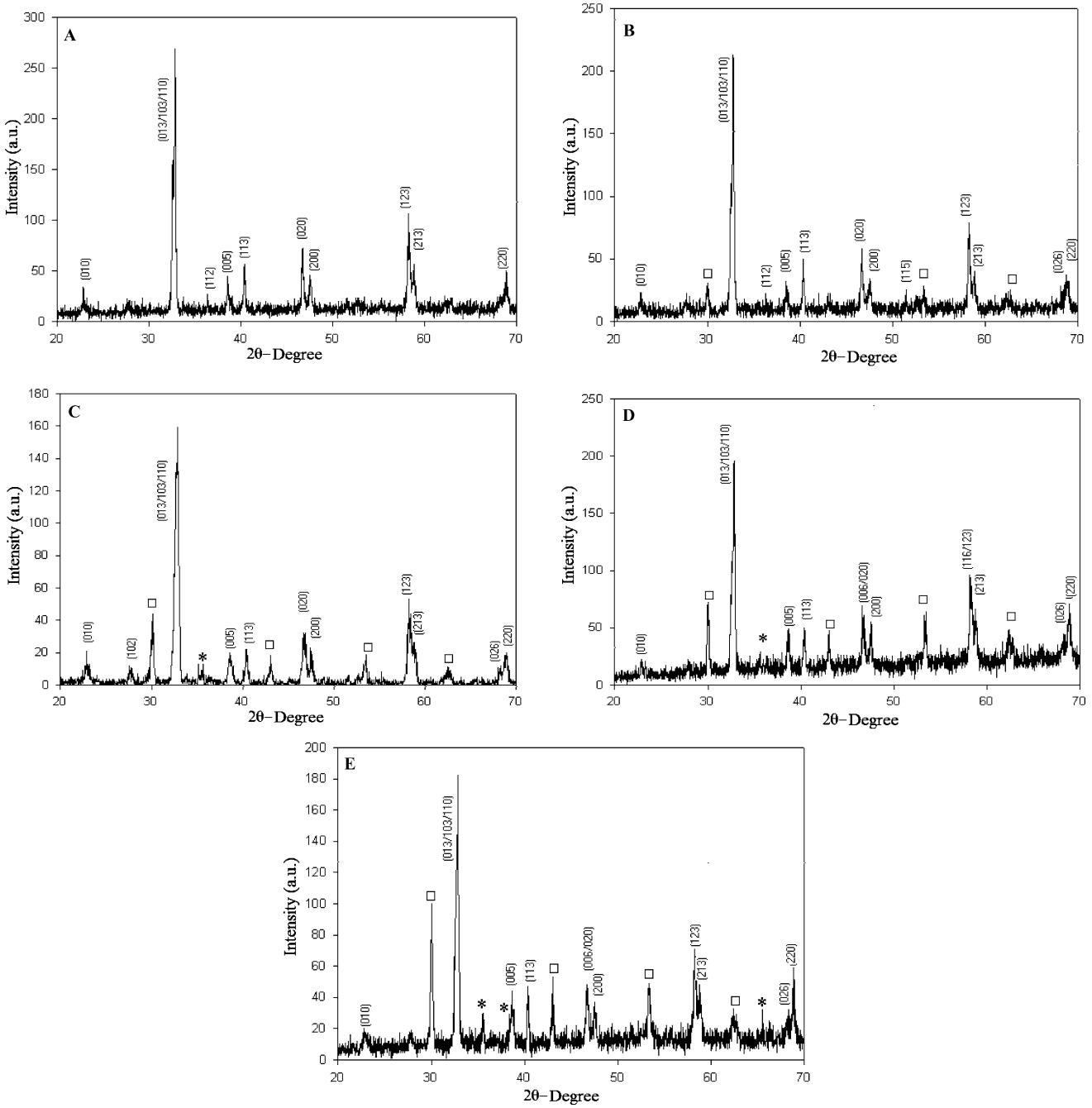

Fig. 8 XRD patterns of samples **A**, **B**, **C**, **D**, and **E** with the composition of $YBa_2Cu_{3-x}Sb_xO_y$ ($x = 0.00$–0.20) (□ YBa_2SbO_6 phase, ∗ CuO phase)

3.2 System II

In this section, results obtained from the effect of Sb substitution for Cu in $YBa_2Cu_{3-x}Sb_xO_y$ with $x = 0.05$, 0.10, 0.15 and 0.20 are presented and discussed. The XRD patterns for the System II samples given in Fig. 8 show that all the samples have a multiphase nature as in System I. The main peaks of the Y123 were observed in all samples. In the lattice parameters which are obtained from the powder diffraction program, were observed small differences. The CuO phase was detected at $2\theta = 35.50°$ in samples C, D, and E. Non-superconducting YBa_2SbO_4 phases were detected in both systems at the same 2θ values. The intensity of the XRD peaks increases with increasing Sb dopant as in the case of System I. However, non-superconducting phases in System II exhibit lower intensities than the samples in System I. These results also confirm the study reported by Paulose et al. [22]. The intensities of the (112) peaks, which

Table 2 The critical temperatures ($T_{c,(onset)}$–$T_{c,(R=0)}$), lattice parameters, oxygen content, density (ρ) and porosity (P) of the $YBa_2Cu_{3-x}Sb_xO_y$ ($0 \le x \le 0.20$) samples

System II x	$T_{c,(onset)}$ (K)	$T_{c,(R=0)}$ (K)	$y(c)$	ρ (g/cm^3)	P (%)
0.00	92	88	6.995	5.77	9.27
0.05	90	84	6.995	5.98	6.00
0.10	–	–	6.992	5.92	6.81
0.15	84	–	6.994	5.71	10.23
0.20	80	–	6.994	5.65	11.07

have a crucial role on the superconductivity in the Y123 system, decrease significantly with Sb doping. The decrease of T_c in sample C, D, and E can be attributed to the suppression of the superconducting phase. Moreover, the $BaCuO_2$ impurity phases, generally observed in the Y123 superconductors prepared by the solid-state reaction method and located at 29° in the XRD patterns of System I samples were not observed in the System II superconductors. The lattice parameters a, b and c, obtained from XRD analysis for all the samples in System II are given in Table 2. It was found that lattice parameters a and b remain unchanged with increasing level of Sb substitution, while a small increase (especially in sample C) was obtained for parameter c. This may be related to the fact that Cu^{2+} ions with a 0.72 Å ionic radius were partially substituted by the Sb^{3+} ions with a larger radius of 0.76 Å. The oxygen concentrations in the unit cells of all the samples in System II were calculated to be approximately 7.0. Such a high oxygen concentration suggests that the Sb^{3+} ions tend to occupy the nearby Cu(1)-O chain sites, thus replacing the Cu atoms and enhancing the oxygen concentration in these regions. In addition, Sb^{3+} ions partially replace Cu^{1+} sites in both systems, while subtracting copper in the second case has affected the Cu(2)-O planes. Generally, the cation doping in YBCO modifies the charge distribution and the lattice structure, which causes a decrease in the critical temperature of the system [24].

The real parts of the AC susceptibility curves for System II are shown in Fig. 9. The magnetic susceptibility-temperature curves (χ–T) clearly show two drops for sample B, while the diamagnetic transition covers a wider temperature range. The critical intergrain temperatures ($T_{c,(onset)}$) for samples A, B, D, and E have been measured as 92, 90, 84, and 80 K, respectively. However, sample C did not show any transition down to liquid nitrogen temperature (77 K). The critical temperatures obtained from AC susceptibility measurements for the System II samples are smaller than those for the System I samples. This can be an identification of the importance of the $BaCuO_2$ impurity phases for the mechanism of superconductivity in the Y123 system.

The SEM micrographs of the System II samples taken at 8000-X magnification are shown in Fig. 10. All the samples have a granular structure with pores between the grains. Sample A with no Sb substitution has a homogeneous microstructure with plate- and needle-like grains. Needle-like grains, which are known to have severe negative effects on critical temperature, became more evident especially in sample B. Also, it is clear that the fracture surface of sample C possesses a denser structure than the top surface. The presence of CuO phase has been determined by the EDAX analysis in samples C, D, and E, while sample C, which has the largest density, contains the highest level of CuO (Fig. 11). The YBa_2SbO_6 phase has been also determined as a second additional impurity phase from the EDAX analysis of samples C, D, and E (Figs. 11–12). The significant increase of pores between the grains has been observed in samples D and E (Fig. 12). The porous structure and irregular second phase particles can be the reason for T_c reduction with Sb addition to System II samples.

The $T_{c,(onset)}$, $T_{c(R=0)}$ critical temperatures, lattice parameters, oxygen contents, densities, and porosities for the System II samples are listed in Table 2. The densities of the System II samples were measured as 90.77%, 94.07%, 93.13%, 89.82%, and 88.88% of the theoretical density of Y123 (6.357 g/cm^3) for $x = 0.00, 0.05, 0.10, 0.15, 0.20$, respectively, and it is shown that there is not a linear relation between the density and the substitution level, from Fig. 13. Samples B and C had larger densities, while D and E possess smaller densities than sample A with no Sb substitution. The partial substitution of Sb^{3+} ions with a 0.76 Å ionic radius for the Cu^{2+} ions with an 0.72 Å ionic radius or the new phases filling the pores in the Y123 system should be the crucial factors for the results above. The dependence of porosity on Sb substitution content is also given in Fig. 13. Pellets D and E possess highly porous microstructures with 10.23% and 11.07% porosities, respectively, while samples B and C have denser structures in agreement with the density, EDAX and SEM analysis.

4 Conclusion

In this study, the effects of Sb substitution at both the Y and Cu sites on the characteristic properties of the Y123 system

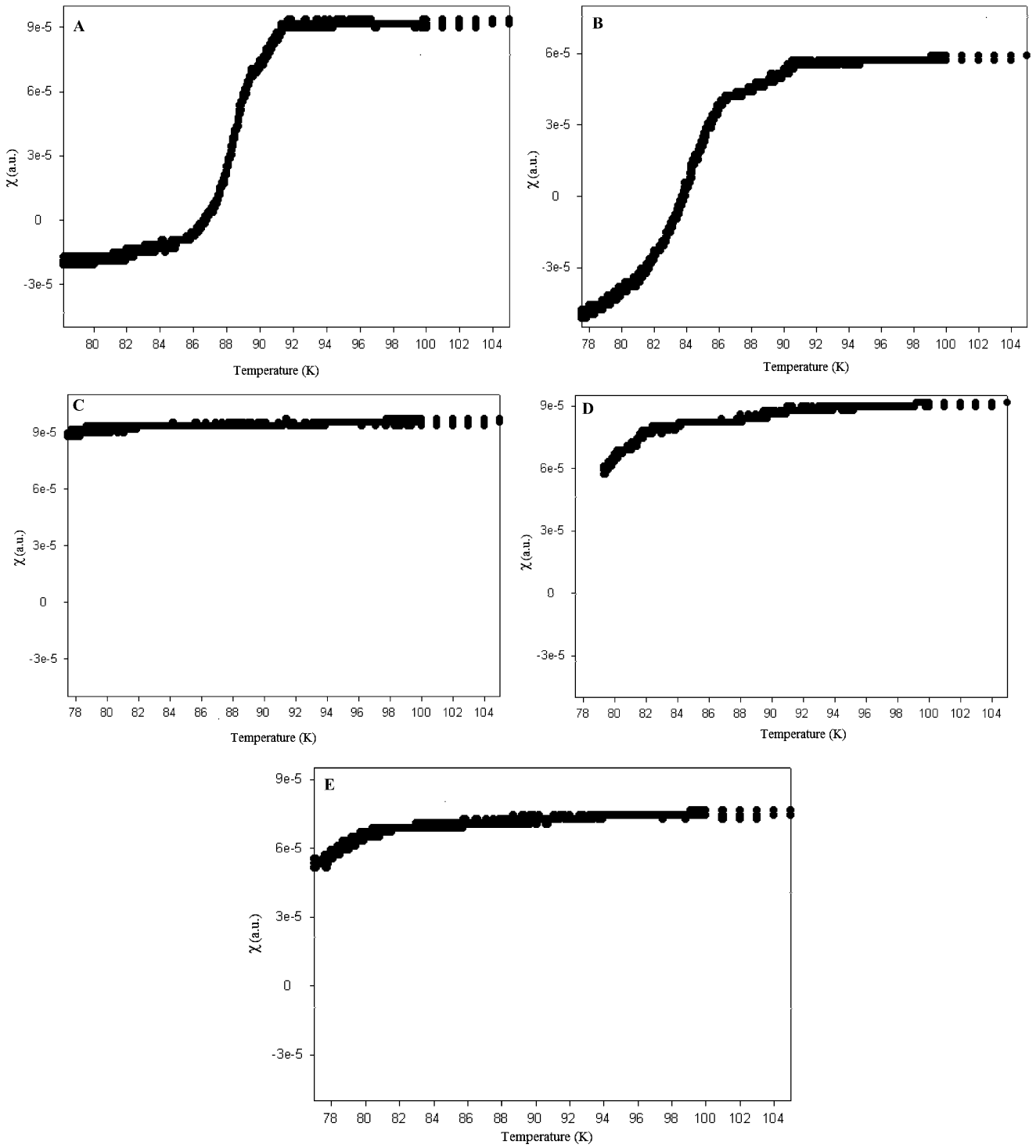

Fig. 9 Temperature dependence of the real part AC susceptibility of the samples $YBa_2Cu_{3-x}Sb_xO_y$ $(0.05 \leq x \leq 0.20)$

which is bulk form were reported. We prepared the samples by the conventional solid-state reaction method and a relatively high critical temperature (∼90–92 K) has been obtained to be in agreement with reported studies on Y123 [2, 18, 24]. The samples were characterized by AC magnetic susceptibility, XRD, SEM, EDAX, and density measurements. From our results, we found that the structures of the $Y_{1-x}Sb_xBa_2Cu_3O_y$ and $YBa_2Cu_{3-x}Sb_xO_y$ samples remain orthorhombic up to the highest doping concentrations. The results of this study also indicated that the realization of thermal treatment in oxygen enriched atmosphere was not crucial for the preparation of pure Y123 unlike some of the

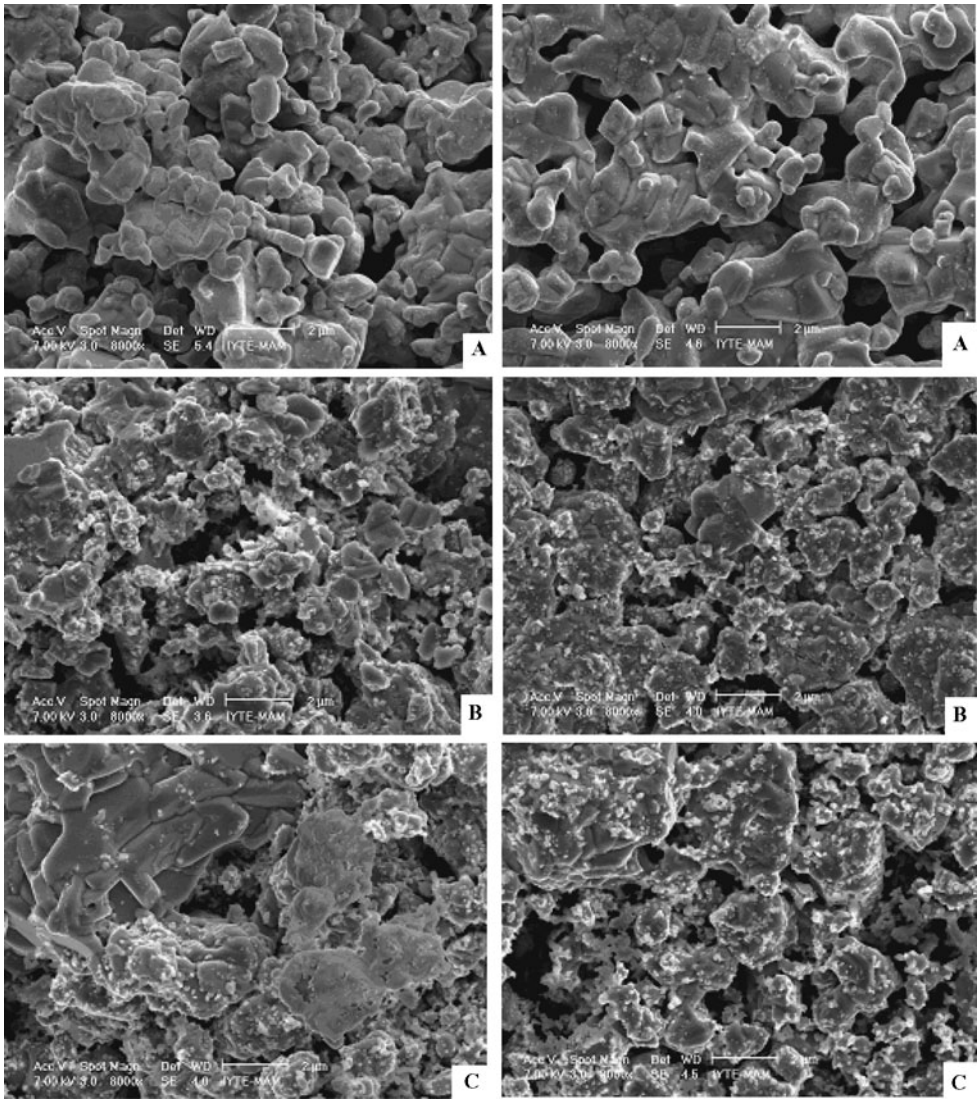

Fig. 10 SEM images of samples $YBa_2Cu_{3-x}Sb_xO_y$ with (**A**) $x = 0.00$, (**B**) $x = 0.05$, (**C**) $x = 0.10$, (**D**) $x = 0.15$, and (**E**) $x = 0.20$ respectively. *Left column* shows the fracture surface while the *right column* shows top surface of samples

previous reports in the literature. In our measurements, the most commonly reported critical temperature value which is approximately 92 K was determined for the pure Y123 sample, although all heat treatments were treated in air atmosphere. In fact, the oxygen content in Y123 superconductors is known to be quite sensitive not only to the oxygen pressure during sintering but also to annealing temperature, annealing time, and cooling rate. So, we concluded that an oxygen flow during heating treatments was neither a necessary nor an adequate factor in order to obtain high oxygen content ($y \sim 7$) as well as high critical temperature in YBCO-based superconductors. The lattice parameter-c and critical temperature were not determined to be closely related unlike the commonly reported dependence of the corresponding properties.

In general, an increase in Sb substitution ratio leads to a decrease in the critical temperature of Y123. However, the Sb substitution of Cu suppressed the critical temperature more effectively than the partial substitution of Sb for Y in the Y123 system. This result emphasizes once more the important role of Cu atoms in the superconductivity mechanism in high-T_c superconductors. The deterioration effect of Sb doping on the superconductivity of Y123 was observed to be almost inversely proportional to the substitution content. Sb substitution in the systems at different ratios leads to the formation of the nonsuperconducting YBa_2SbO_6 phase. In addition, the pellets have porous structures with porosities in the ranges of 7.42%–11.97% and 6.00%–11.07% for Systems I and II, respectively. We believe that the Sb doping fills the pores (up to a threshold) and causes the formation of denser samples. This can be connected with improvements in the weak links at the grain boundaries, which can be attributed to the smaller reduction of critical temperature obtained for Y123 superconductors after being partial substituted with a large enough amount of Sb dopant.

Fig. 10 (*Continued*)

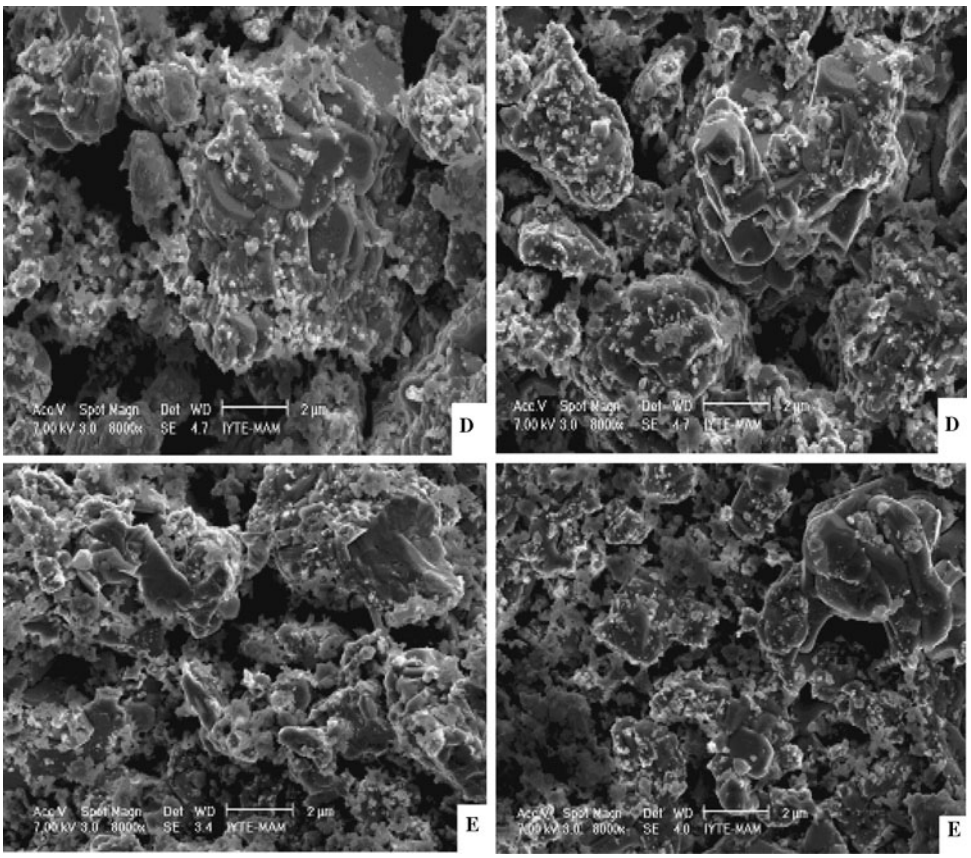

Fig. 11 (Color online) EDAX analysis for two different regions of C sample ($x = 0.10$) in the System II

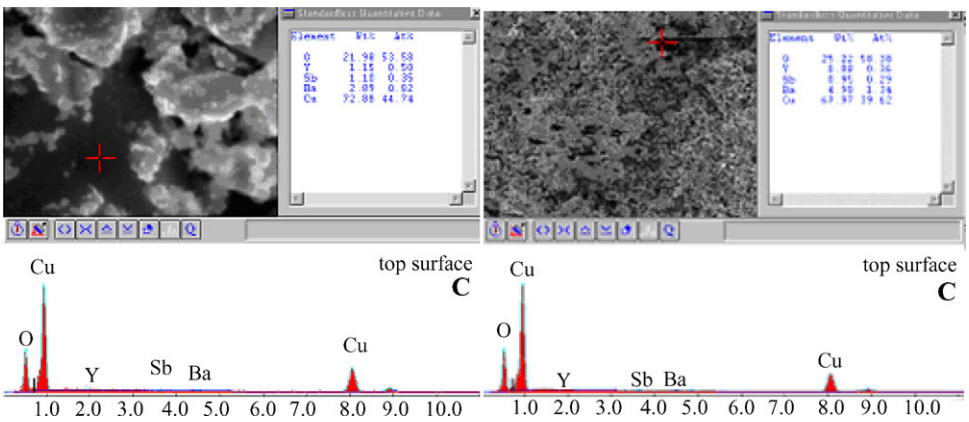

Fig. 12 (Color online) EDAX analysis results for **D** ($x = 0.15$) and **E** ($x = 0.20$) samples of $YBa_2Cu_{3-x}Sb_xO_y$ system

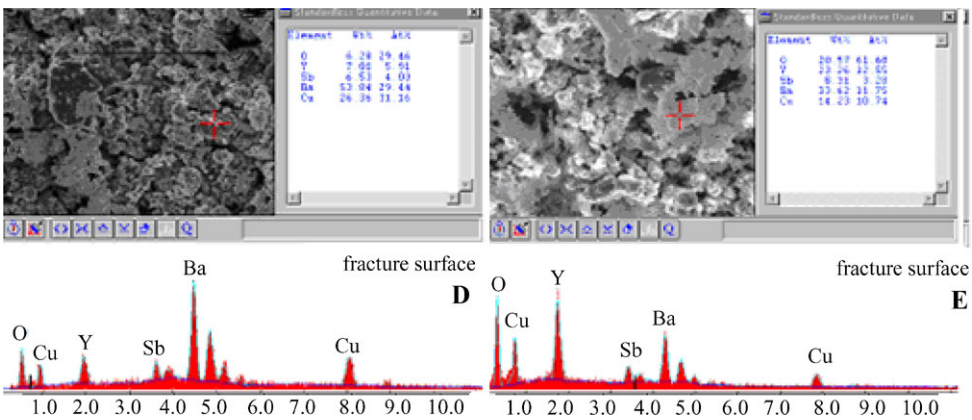

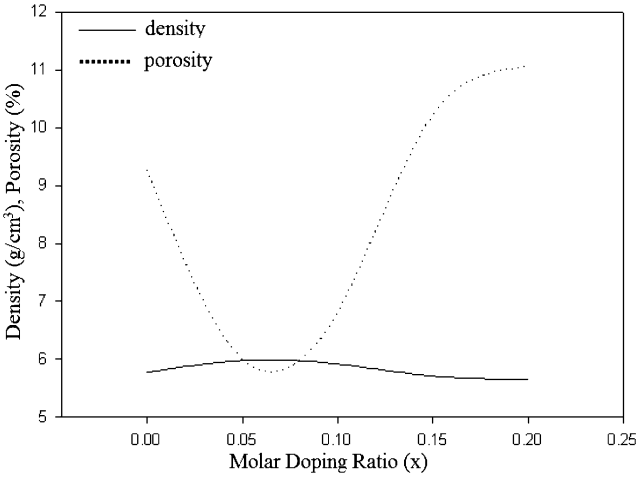

Fig. 13 Variation of the density and porosity of Sb doped $YBa_2Cu_{3-x}Sb_xO_y$ ($0 \leq x \leq 0.20$) samples

One could conclude that Sb_2O_3 substitution in Y123 system lead to weaker connectivity between superconducting grains and loose its superconducting characteristic.

References

1. Bednorz, J.G., Muller, K.A.: Z. Phys. B **64**, 189 (1986)
2. Wu, K., Ashburn, J.R., Torng, C.J., Hor, P.H., Meng, R.L., Gao, L., Huang, Z.J., Wang, Y.Q., Chu, C.W.: Phys. Rev. Lett. **58**, 908 (1987)
3. Marsh, P., Fleming, R.M., Mandich, M.L., DeSantolo, A.M., Kwo, J., Hong, M., Martinez-Miranda, L.J.: Nature **334**, 660 (1988)
4. Bordet, P., Chaillout, C., Chenavas, J., Hodeau, J.L., Marezio, M., Karpinski, J., Kaldis, E.: Nature **336**, 596 (1988)
5. Öztürk, A., Düzgün, İ., Çelebi, S.: J. Alloys Compd. **495**, 104–107 (2010)
6. Udomsamuthirun, P., Kruaehong, T., Nilkamjon, T., Ratreng, S.: J. Supercond. Nov. Magn. (2010). doi:10.1007/s10948-010-0786-9
7. Wei, G., Guisheng, Z., Xiao, C., Aiping, W., Jiarun, H., Hailin, B., Jialie, R., Yulei, J.: Physica C **470**, 482–486 (2010)
8. Zheng, M.H., Xiao, L., Ren, H.T., Jiao, Y.L., Chen, Y.X.: Physica C **386**, 258–261 (2003)
9. Lee, S.H., Choi, Y.: Physica B **404**, 734–736 (2009)
10. Pinheiro, L., Jurelo, A., Serbena, F., Rodrigues, P. Jr., Foerster, C., Chinelatto, A.: Physica C **470**, 465–469 (2010)
11. Aliabadi, A., Farschi, Y.A., Akhavan, M.: Physica C **469**, 2012–2014 (2009)
12. Bilgili, O., Selamet, Y., Kocabas, K.: J. Supercond. Nov. Magn. **21**, 439–449 (2008)
13. Kocabas, K., Bilgili, O., Yasar, N.: J. Supercond. Nov. Magn. **22**, 643–650 (2009)
14. Kocabas, K., Sakiroglu, S., Ciftcioglu, M., Ercan, I., Epik, H., Bilgili, O.: J. Supercond. Nov. Magn. **22**, 749–754 (2009)
15. Kocabas, K., Ozkan, O., Bilgili, O., Kadioglu, Y., Yilmaz, H.: J. Supercond. Nov. Magn. **23**, 1485–1492 (2010)
16. Koutzarova, T., Nedkov, I., Ausloos, M., Cloots, R., Midlarz, T., Nogues, M.: Phys. Status Solidi (a) **191**, 235–242 (2002)
17. Khosroabadi, H., Mohammadi Zadeh, M.R., Akhavan, M.: Physica C **370**, 85–93 (2002)
18. Kocabaş, K., Kazancı, N., Tepe, M.: Turk. J. Phys. **22**, 65–68 (1998)
19. Lin, T.X., Zhang, J.L., Ren, H.T., He, Q., Xiao, L., Yin, D.: J. Phys., Condens. Matter **3**, 6875–6880 (1991)
20. Jin, S., Tiefel, T.H., Fastnacht, R.A., Kammlott, G.W.: Appl. Phys. Lett. **60**, 3307 (1992)
21. Vlakhov, E., Gattef, E., Dimitriev, Y., Staneva, A.: J. Mater. Sci. Lett. **13**, 1654–1656 (1994)
22. Paulose, K.V., Koshy, J., Uma Devi, P., Damodaran, A.D.: Appl. Phys. Lett. **59**, 1251–1253 (1991)
23. Saha, S., Tripathi, R.B., Das, B.K.: Supercond. Sci. Technol. **5**, 703–706 (1992)
24. Skakle, J.M.S.: Mater. Sci. Eng. **R23**, 1–40 (1998) (Invited Review)
25. Lee, S.H., Choi, Y.: Physica B **404**, 734 (2009)
26. Li, A., Wang, Y.N., Ying, X.N., Zhang, Q.M., Chen, W.M.: Supercond. Sci. Technol. **12**, 645 (1999)
27. Bell, A.M.T.: Supercond. Sci. Technol. **3**, 55–61 (1990)
28. Kistenmacher, T.J.: J. Appl. Phys. **64**, 5067–5070 (1988)
29. Poole, C.J., Farach, H.A., Creswick, R.: Superconductivity, pp. 320–321. Academic Press, San Diego (1995)
30. Ravinder Reddy, R., Murakami, M., Tanaka, S., Venugopal Reddy, P.: Physica C **257**, 137–142 (1996)